CHEMISTRY
A EUROPEAN JOURNAL

DOI: 10.1002/chem.200700619

Gas-Phase Reactivity of Metavanadate $[VO_3]^-$ towards Methanol and Ethanol: Experiment and Theory

Tom Waters,*[a, b] Anthony G. Wedd,[a, b] and Richard A. J. O'Hair*[a, b]

Abstract: The gas-phase reactivity of the metavanadate anion $[VO_3]^-$ towards methanol and ethanol was examined by a combination of ion–molecule reaction and isotope labelling experiments in a quadrupole ion-trap mass spectrometer. The experimental data were interpreted with the aid of density functional theory calculations. $[VO_3]^-$ dehydrated methanol to eliminate water and form $[VO_2(\eta^2\text{-}OCH_2)]^-$, which features an $[\eta^2\text{-}C,O\text{-}OCH_2]^{2-}$ ligand formed by formal removal of two protons from methanol and which is isoelectronic with peroxide. $[VO_3]^-$ reacted with ethanol in an analogous manner to form $[VO_2(\eta^2\text{-}OCHCH_3)]^-$, as well as by loss of ethene to form $[VO_2(OH)_2]^-$. The calculations predicted that important intermediates in these reactions were the hydroxo alkoxo anions $[VO_2(OH)(OCH_2R)]^-$ (R: H, CH_3). These were predicted to undergo intramolecular hydrogen-atom transfer to form $[VO(OH)_2(\eta^1\text{-}OCHR)]^-$ followed by $\eta^1\text{-}O \rightarrow \eta^2\text{-}C,O$ rearrangements to form $[VO(OH)_2(\eta^2\text{-}OCHR)]^-$. The latter reacted further to eliminate water and generate the product $[VO_2(\eta^2\text{-}OCHR)]^-$. This major product observed for $[VO_3]^-$ is markedly different from that observed previously for $[NbO_3]^-$ containing the heavier Group 5 congener niobium. In that case, the major product of the reaction was an ion of stoichiometry $[Nb, O_3, H_2]^-$ arising from the formal dehydrogenation of methanol to formaldehyde. The origin of this difference was examined theoretically and attributed to the intermediate alkoxo anion $[NbO_2(OH)(OCH_3)]^-$ preferring hydride transfer to form $[HNbO_2(OH)]^-$ with loss of formaldehyde. This contrasts with the hydrogen-atom-transfer pathway observed for $[VO_2(OH)(OCH_3)]^-$.

Keywords: alcohols · gas-phase reactions · hydrogen transfer · oxidation · vanadates

Introduction

Transition-metal-oxide catalysts are employed in a variety of catalytic oxidation processes of significant importance to global chemical industries.[1] A quarter of the most important organic chemicals are produced by heterogeneous oxidation catalysis, and more than a third of worldwide catalyst production is based on oxides.[2] Bulk or supported vanadium oxides are important in a number of heterogeneous catalytic reactions and are the focus of sustained research efforts.[3–5] They are employed as catalysts for reactions such as the oxidation of sulfur dioxide to sulfur trioxide, butane to maleic anhydride and methanol to formaldehyde.[3–5] In addition, discrete vanadium–oxo and –peroxo centres are active in many oxidation reactions observed in solution.[6,7]

The molecular structure and reactivity of active sites on metal-oxide catalysts has been a particular focus.[1–5,8–11] However, detailed mechanistic studies are often hampered by factors such as the dynamic nature of the catalyst surface and its inhomogeneity. Furthermore, important reactions appear to occur at localized reaction sites (such as surface defects or adsorbed reactant molecules), and such sites might exhibit significantly different reactivity from that of the bulk oxide. A proper understanding of these differences is vital in order to understand their specific functions.

Gas-phase studies of isolated transition-metal-oxide cluster ions can provide molecular-level insights into the fundamental reactivity of clusters of known stoichiometry under well-defined experimental conditions.[12,13] Such insights can help us to understand related reactions occurring at oxide

[a] Dr. T. Waters, Prof. A. G. Wedd, Prof. R. A. J. O'Hair
School of Chemistry
The University of Melbourne
Melbourne, Victoria 3010 (Australia)
E-mail: waterst@unimelb.edu.au

[b] Dr. T. Waters, Prof. A. G. Wedd, Prof. R. A. J. O'Hair
Bio21 Institute of Molecular Science and Biotechnology
The University of Melbourne
Melbourne, Victoria 3010 (Australia)
Fax: (+613) 9347-5180

Supporting information for this article is available on the WWW under http://www.chemeurj.org/ or from the author.

surfaces. Accordingly, a primary aim is to identify new modes of reactivity and bonding in the gas phase that might be relevant to condensed-phase chemistry. To this end, the reactivity of a range of cationic and anionic vanadium oxide centres towards neutral reagents, such as alkanes, alkenes and alcohols, has been examined.[14–28] In particular, studies of the reactivity of the vanadium oxide cluster ions with alcohols is driven by the industrial applications of heterogeneous vanadium oxide catalysts in the oxidation of methanol, and the likely intermediacy of vanadium alkoxide species in other oxidation reactions mediated by vanadium oxides.[25–32] Heavier niobium and tantalum gas-phase clusters have also been examined,[25,26,29,33–37] again in the context of the catalytic application of niobium and tantalum oxide surfaces.[38,39] The majority of these gas-phase studies have been supported by theoretical calculations.[26,27,31,32,40–42]

We recently described the gas-phase catalytic oxidation of methanol to formaldehyde with the mononuclear metavanadate anion $[VO_3]^-$ as catalyst and dioxygen as terminal oxidant.[28] The $2e^-$ oxidation of the alcohol was linked to the $4e^-$ reduction of dioxygen. A key step in the process was the reaction of $[VO_3]^-$ with methanol to eliminate water and form $[VO_2(\eta^2\text{-}OCH_2)]^-$, with an $[\eta^2\text{-}O,C\text{-}OCH_2]^{2-}$ ligand which may be regarded formally as doubly deprotonated methanol or as $2e^-$-reduced formaldehyde. This ligand is isolelectronic with the peroxo ligand O_2^{2-}, and was crucial in linking the $2e^-$ oxidation of two equivalents of methanol to the $4e^-$ reduction of dioxygen.[28]

Herein, we describe aspects of the reaction of $[VO_3]^-$ and methanol in more detail, and include the equivalent reaction with ethanol. Reaction pathways were examined by kinetic and isotope labelling experiments, and experimental data were interpreted with the aid of detailed density functional theory (DFT) calculations. The reaction of $[VO_3]^-$ with methanol follows a different course to that reported previously for $[NbO_3]^-$,[36] and likely explanations for this difference are offered. Finally, the relevance of the present observations to the mechanism of similar reactions at metal-oxide surfaces is discussed.

Results and Discussion

Electrospray ionization of $NaVO_3$ in acetonitrile/water solutions provided access to the metavanadate anion $[VO_3]^-$ and the dihydroxodioxo anion $[VO_2(OH)_2]^-$.[43–46] Polynuclear oxovanadium centres were also observed (e.g. $[V_2O_7]^{2-}$ and $[V_3O_8(OH)]^{2-}$) but are not discussed here. The present work describes the gas-phase reactivity of the anion $[VO_3]^-$ towards methanol and ethanol. Relevant spectra are presented in Figures 1 and 2, respectively, and summarized in Table 1, while schemes outlining the observed reactions and m/z values of relevant species are included in Scheme 1.

Reaction of $[VO_3]^-$ with methanol: Spectra for the reaction of $[VO_3]^-$ and methanol are presented in Figure 1. The observed reactions are summarized in Table 1, Scheme 1a and Equation (1). $[VO_3]^-$ (m/z: 99) reacted with methanol to form the major product ion at m/z: 113 of stoichiometry [V, O_3, C, H_2]$^-$ with loss of neutral water [Eq. (1b)]. A product ion at m/z: 101 of stoichiometry [V, O_3, H_2]$^-$ arising from

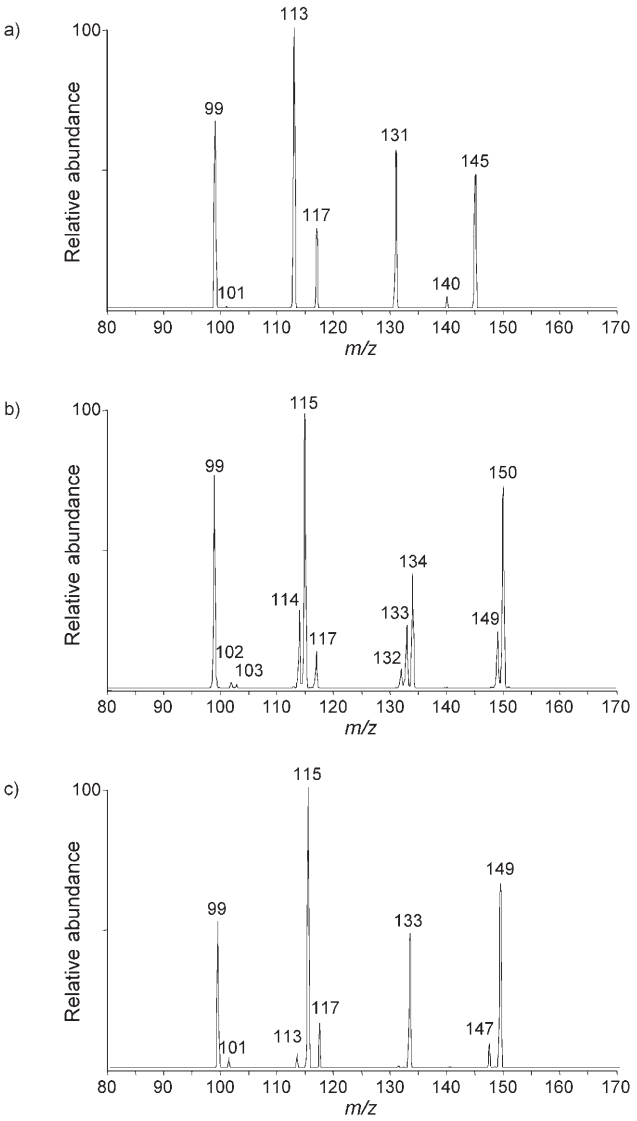

Figure 1. Mass spectra illustrating reaction of $[VO_3]^-$ (m/z: 99) with methanol ($c = \approx 1\times10^{10}$ molecules cm^{-3}, reaction time = 30 ms). The peaks at m/z: 117 and 140 are assigned to addition of background H_2O and CH_3CN, respectively, to m/z: 99. a) Reaction with CH_3OH to form [V, O_3, H_2]$^-$ (m/z: 101), $[VO_2(\eta^2\text{-}OCH_2)]^-$ (m/z: 113) and $[VO_2(OH)(OCH_3)]^-$ (m/z: 131). Some of the signal at m/z: 131 is also due to addition of water to m/z: 113, while the signal at m/z: 145 is due to the addition of CH_3OH to m/z: 113. b) Reaction with CD_3OH to form [V, O_3, H, D]$^-$, [V, O_3, D_2]$^-$ (m/z: 102 and 103, respectively), $[VO_2(\eta^2\text{-}OCHD)]^-$, $[VO_2(\eta^2\text{-}OCD_2)]^-$ (m/z: 114 and 115, respectively) and $[VO_2(OH)(OCD_3)]^-$ (m/z: 134). The signals at m/z: 132/133 and m/z: 149/150 are from the addition of H_2O and CD_3OH, respectively, to m/z: 114/115. c) Reaction with $CH_3{}^{18}OH$ to form [V, O_3, H_2]$^-$ (m/z: 101), $[VO_2(\eta^2\text{-}{}^{18}OCH_2)]^-$ (m/z: 115) and $[VO_2(OH)({}^{18}OCH_3)]^-$ (m/z: 133). Some of the signal at m/z: 133 is also due to the addition of water to m/z: 115, while the signal at m/z: 149 is due to the addition of $CH_3{}^{18}OH$ to m/z: 115. The weak peaks at m/z: 113 and 147 are due to $CH_3{}^{16}OH$ impurity in the $CH_3{}^{18}OH$ sample (95% atom ^{18}O).

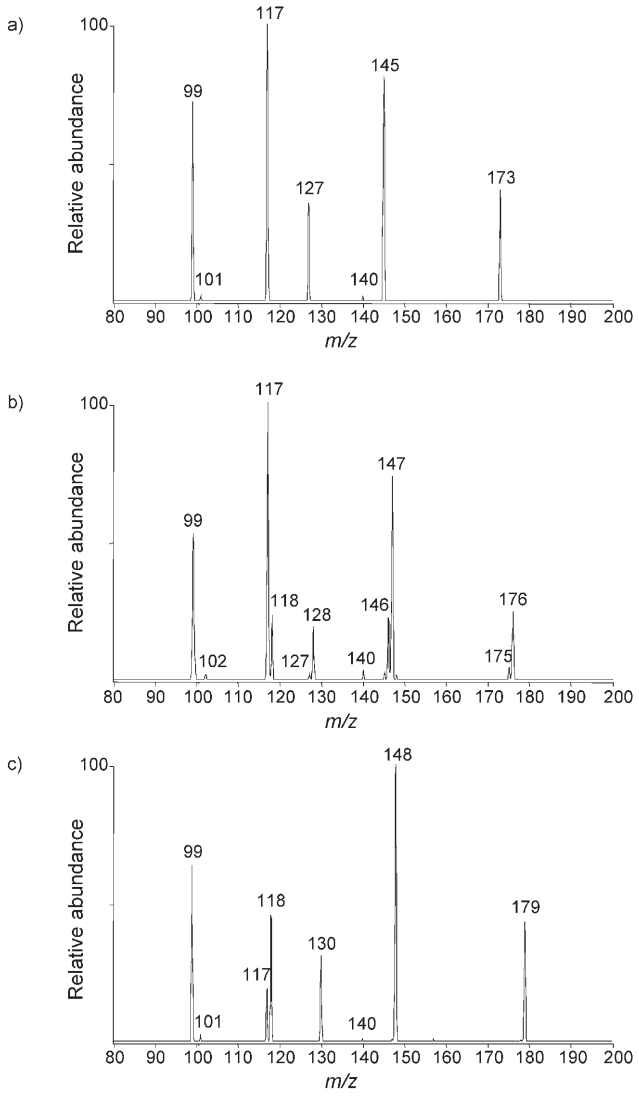

Figure 2. Mass spectra illustrating the reaction of $[VO_3]^-$ (m/z: 99) with ethanol ($c = \approx 1 \times 10^{10}$ molecules cm^{-3}, reaction time = 30 ms). Some of the signal at m/z: 117 is due to the addition of background H_2O to m/z: 99, while the signal at m/z: 140 is due to addition of background CH_3CN to m/z: 99. a) Reaction with CH_3CH_2OH to form $[V, O_3, H_2]^-$ (m/z: 101), $[VO_2(OH)_2]^-$ (m/z: 117), $[VO_2(\eta^2\text{-}OCHCH_3)]^-$ (m/z: 127) and $[VO_2(OH)(OCH_2CH_3)]^-$ (m/z: 145). Some of the signal at m/z: 145 is also due to the addition of background H_2O to m/z: 127, while the signal at m/z: 173 is due to the addition of CH_3CH_2OH to m/z: 127. b) Reaction with CH_3CD_2OH to form $[V, O_3, H, D]^-$ (m/z: 102), $[VO_2(OH)_2]^-$ and $[VO_2(OH)(OD)]^-$ (m/z: 117 and 118, respectively), $[VO_2(\eta^2\text{-}OCHCH_3)]^-$ and $[VO_2(\eta^2\text{-}OCDCH_3)]^-$ (m/z: 127 and 128, respectively) and $[VO_2(OH)(OCD_2CH_3)]^-$ (m/z: 147). The signals at m/z: 145/146 and m/z: 175/176 are from the addition of H_2O and CH_3CD_2OH, respectively, to m/z: 127/128. c) Reaction with CD_3CH_2OH to form $[V, O_3, H_2]^-$ (m/z: 101), $[VO_2(OH)(OD)]^-$ (m/z: 118), $[VO_2(\eta^2\text{-}OCHCD_3)]^-$ (m/z: 130) and $[VO_2(OH)(OCH_2CD_3)]^-$ (m/z: 148). The signal at m/z: 117 is due to the addition of background H_2O to m/z: 99. Some of the signal at m/z: 148 is also due to the addition of background H_2O to m/z: 130, while the signal at m/z: 179 is due to the addition of CD_3CH_2OH to m/z: 130.

loss of neutral formaldehyde was also observed, but with much lower yield [Eq. (1a)]. Some of the signal at m/z: 131 arises from direct addition of methanol to $[VO_3]^-$ (m/z: 99) [Eq. (1c)]. The ions at m/z: 117 and 140 are due to the addition of background water and acetonitrile, respectively, to $[VO_3]^-$, while the ions at m/z: 131 and 145 arise from secondary reactions involving addition of water and methanol, respectively, to the primary product ion at m/z: 113 (Figure 1a). Each of the secondary reactions was verified independently by multistage mass spectrometry (MS^3) experiments (data not shown).

Table 1. Observed primary product ions, neutral losses and branching ratios for ion–molecule reactions of $[VO_3]^-$ with labelled methanol and ethanol. See also Figures 1 and 2 and Scheme 1.

Neutral reagent	Product ion (m/z)	Neutral loss	Branching ratio [%][a]
CH_3OH[b]	101	$-H_2CO$	1
	113	$-H_2O$	99
CD_3OH	102	$-D_2CO$	1
	103	$-DHCO$	1
	114	D_2O	22
	115	DHO	76
$CH_3{}^{18}OH$	101	$-H_2C^{18}O$	2
	115	$-H_2{}^{16}O$	98
CH_3CH_2OH[b]	101	$-CH_3CHO$	1
	117	$-CH_2CH_2$	44
	127	$-H_2O$	55
CH_3CD_2OH	102	$-CH_3CDO$	1
	117	$-CH_2CD_2$	45
	118	$-CH_2CDH$	13
	127	$-D_2O$	6
	128	$-DHO$	35
CD_3CH_2OH	101	$-CD_3CHO$	2
	118	$-CD_2CH_2$	31
	130	$-H_2O$	67

[a] Intensities are normalized to sum of 100%. Direct addition of the alcohol to $[VO_3]^-$ is not included in branching ratios. Intensities were corrected to account for secondary reactions with alcohol and background water (see Scheme 1). [b] Rates of reaction with CH_3OH and CH_3CH_2OH were measured as 2.5 and 2.7×10^{-9} molecule cm^{-3} s^{-1}, respectively, corresponding to unit efficiency.

$$[VO_3]^- \ (m/z: \ 99) + CH_3OH \rightarrow [V, O_3, H_2]^- \ (m/z: \ 101) + CH_2O \quad (1a)$$

$$\rightarrow [V, O_3, C, H_2]^- \ (m/z: \ 113) + H_2O \quad (1b)$$

$$\rightarrow [VO_2(OH)(OCH_3)]^- \ (m/z: \ 131) \quad (1c)$$

The rate constant for the reaction between $[VO_3]^-$ and methanol was measured as 2.5×10^{-9} molecules cm^{-3} s^{-1}, faster than the calculated ion–molecule collision rate (1.9×10^{-9} molecules cm^{-3} s^{-1}) and corresponding to unit efficiency within experimental error.[47] The rapid formation of $[V, O_3, C, H_2]^-$ (m/z: 113) implies the absence of energetic barriers in the reaction pathway above the energy of the entrance channel $[VO_3]^- + CH_3OH$.

The reaction was also carried out with the labelled methanols CD_3OH and $CH_3{}^{18}OH$ to provide insights into the reaction mechanisms and clarification of the different reaction pathways (Figure 1, Table 1). Reaction with CD_3OH resulted in the predominant loss of DHO to form $[V, O_3, C, D_2]^-$ (m/z: 115), but with some loss of D_2O to form [V, O_3, C, H,

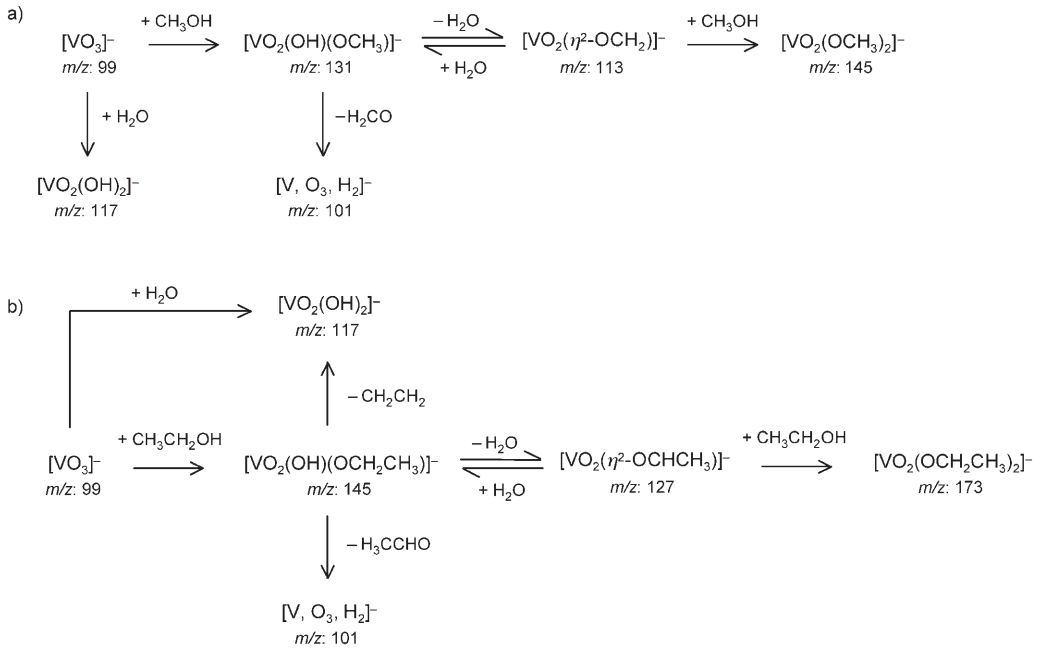

Scheme 1. Reaction schemes summarizing the sequence of reactions observed between $[VO_3]^-$ and a) methanol and b) ethanol.

D]$^-$ (m/z: 114; Figure 1b, Table 1). The predominant loss of neutral DHO indicated that the hydroxyl hydrogen and a methyl deuterium of CD_3OH are incorporated into product water. The observed loss of D_2O indicates some label scrambling and incorporation of two methyl deuterium atoms into product water. The peaks at m/z: 132 and 133 are consistent with addition of background water to the primary products at m/z: 114 and 115, respectively, while the peak at m/z: 134 can only arise from the direct addition of CD_3OH to $[VO_3]^-$ (m/z: 99). The weaker peaks observed at m/z: 102 and 103 are consistent with the loss of both CD_2O and CHDO, and formation of $[V, O_3, H, D]^-$ and $[V, O_3, D_2]^-$, respectively. Losses of CD_2O and CHDO are again consistent with some label scrambling between the hydroxyl hydrogen and methyl deuterium atoms in reactant CD_3OH.

Reaction with $CH_3{}^{18}OH$ resulted in the clean formation of $[V, {}^{16}O_2, {}^{18}O, C, H_2]^-$ (m/z: 115), indicating that the oxygen atom of methanol is retained exclusively on product $[V, O_3, C, H_2]^-$ and that an oxygen atom of parent $[VO_3]^-$ is lost with neutral water (Figure 1c, Table 1). The peak at m/z: 133 is consistent with both the addition of background water to the major product ion at m/z: 115 and/or with direct addition of $CH_3{}^{18}OH$ to $[VO_3]^-$ (m/z: 99).

Reaction of $[VO_3]^-$ with ethanol: The reactivity of $[VO_3]^-$ towards ethanol was examined for comparison with that of methanol, and spectra are presented in Figure 2. The observed reactions are similar to those for methanol, and are summarized in Table 1, Scheme 1b and Equation (2). The product at m/z: 101 is assigned to an ion of stoichiometry $[V, O_3, H_2]^-$ with loss of neutral acetaldehyde [Eq. (2a)]. The ion at m/z: 117 is assigned to $[VO_2(OH)_2]^-$ formed by formal dehydration of ethanol and loss of ethene [Eq. (2b)]. This reaction was not observed for methanol. Although a small component of the signal at m/z: 117 might be formed due to direct addition of background water to $[VO_3]^-$, rate measurements and isotope labelling experiments indicate that the majority is formed from reaction with ethanol (Figure 2b,c). The product ion at m/z: 127 of stoichiometry $[V, O_3, C_2, H_4]^-$ arises from formal dehydration of ethanol [Eq. (2c)], and is presumably analogous to product $[V, O_3, C, H_2]^-$ (m/z: 113) generated from reaction with methanol. Finally, the product ion at m/z: 145 arises from the direct addition of ethanol to $[VO_3]^-$ [Eq. (2d)] and from the addition of background H_2O to the primary product at m/z: 127.

$$[VO_3]^- \ (m/z:\ 99) + CH_3CH_2OH \rightarrow [V, O_3, H_2]^- \ (m/z:\ 101) + CH_3CHO \quad (2a)$$

$$\rightarrow [VO_2(OH)_2]^- \ (m/z:\ 117) + C_2H_4 \quad (2b)$$

$$\rightarrow [V, O_3, C_2, H_4]^- \ (m/z:\ 127) + H_2O \quad (2c)$$

$$\rightarrow [VO_2(OH)(OCH_2CH_3)]^- \ (m/z:\ 145) \quad (2d)$$

The rate constant for the reaction between $[VO_3]^-$ and ethanol was measured as 2.7×10^{-9} molecules cm^{-3}s^{-1}, again faster than the calculated ion–molecule collision rate constant (1.9×10^{-9} molecules cm^{-3}s^{-1}) and corresponding to unit efficiency within experimental error.[47] The rapid rate implies the absence of energetic barriers in the reaction pathway above the energy of the entrance channel $[VO_3]^- + CH_3CH_2OH$.

The reaction was also carried out with the labelled ethanols CH_3CD_2OH and CD_3CH_2OH (Table 1, Figure 2). Reaction with CH_3CD_2OH resulted in the loss of CH_2CD_2 and

CH_2CDH to form ions $[VO_2(OH)_2]^-$ and $[VO_2(OH)(OD)]^-$ at m/z: 117 and 118, respectively (Figure 2b, Table 1). Loss of CH_2CDH suggests exchange of hydroxyl hydrogen and methylene deuterium atoms of CH_3CD_2OH prior to loss of ethene, consistent with similar observations for CD_3OH. Similarly, product ions observed at m/z: 127 and 128 were consistent with loss of D_2O and DHO to form $[V, O_3, C_2, H_4]^-$ and $[V, O_3, C_2, H_3, D]^-$, respectively, again consistent with exchange prior to loss of water. Reaction with CD_3CH_2OH resulted in product ions at m/z: 117 and 118 (Figure 2c). The latter is assigned to $[VO_2(OH)(OD)]^-$ arising from direct loss of CD_2CH_2, while the ion at m/z: 117 is presumed to arise from direct addition of background water to $[VO_3]^-$ rather than from reaction with CD_3CH_2OH. This assumption was supported by kinetic measurements (formation of ion m/z: 117 independent of CD_3CH_2OH pressure) and by the fact that the product at m/z: 117 was also observed in the reaction with CD_3CD_2OD (data not shown). The product ion at m/z: 130 is assigned to $[V, O_3, C_2, H, D_3]^-$ arising from clean loss of H_2O. The absence of signal m/z: 128/129 indicates no exchange of methyl deuterium atoms of CD_3CH_2OH into neutral water.

Theoretical investigation of observed ions: The products from the reaction of $[VO_3]^-$ and CH_3OH were assigned to ions of stoichiometry $[V, O_3, H_2]^-$ (m/z: 101) and $[V, O_3, C, H_2]^-$ (m/z: 113), resulting from elimination of formaldehyde and water, respectively [Eq. (1a,b)]. Equivalent ions $[V, O_3, H_2]^-$ (m/z: 101) and $[V, O_3, C_2, H_4]^-$ (m/z: 127) were also observed in the reaction with ethanol, from the loss of acetaldehyde and water, respectively [Eq. (2a,c)]. Initial theoretical calculations were aimed at addressing the stability of different structural isomers of these unknown product ions. Results are presented in Figure 3.

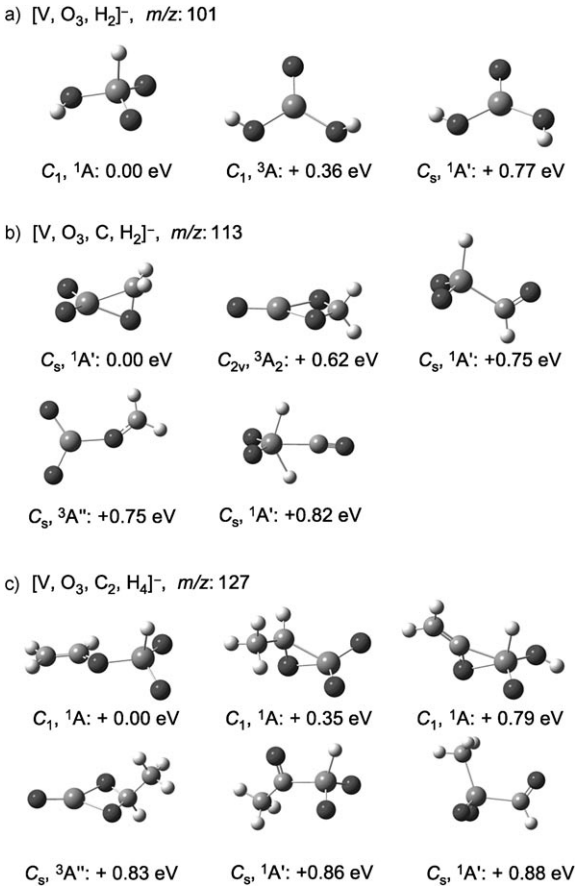

Figure 3. Structures and relative energies (ΔE, eV) for different isomers of ions of stoichiometry: a) $[V, O_3, H_2]^-$ (m/z: 101), b) $[V, O_3, C, H_2]^-$ (m/z: 113) and c) $[V, O_3, C_2, H_4]^-$ (m/z: 127). Energies are relative to the most stable isomer in each case, and only isomers predicted to lie within $\approx$0.8 eV of the most stable isomer are shown.

$[V, O_3, H_2]^-$ (m/z: 101): Two isomers were examined: the anion $[HVO_2(OH)]^-$ with a hydrido ligand (formally $V^V(d^0)$) and singlet and triplet states of the dihydroxo anion $[VO(OH)_2]^-$ (formally $V^{III}(d^2)$). Calculations indicated $[HVO_2(OH)]^-$ was favoured over the triplet state of $[VO(OH)_2]^-$ by 0.36 eV, and over the singlet state by 0.77 eV (Figure 3a).

$[V, O_3, C, H_2]^-$ (m/z: 113): A number of singlet and triplet isomers were considered. The isomer $[V^VO_2(\eta^2\text{-}OCH_2)]^-$ was favoured (Figure 3b). This features an $[\eta^2\text{-}C,O\text{-}OCH_2]^{2-}$ ligand formed by formally removing two protons from methanol, and which is isoelectronic with peroxide. The ligand can also be considered as $2e^-$-reduced formaldehyde. Metric parameters are consistent with such a formulation (e.g. C–O, 1.39 Å; cf. CH_3–OH, 1.42 Å, and CH_2=O, 1.20 Å). This isomer was predicted to be favoured over other singlet and triplet isomers by at least 0.6 eV (Figure 3b).

$[V, O_3, C_2, H_4]^-$ (m/z: 127): Singlet and triplet isomers were considered for this product formed in the reaction of $[VO_3]^-$ and ethanol. The most stable isomer was predicted to be the anion $[HV^VO_2(OCH{=}CH_2)]^-$ containing a hydrido and a vinoxo ligand (Figure 3c). The next most stable isomer was $[V^VO_2(\eta^2\text{-}OCHCH_3)]^-$ (containing the $[\eta^2\text{-}C,O\text{-}OCHCH_3]^{2-}$ ligand), which was predicted to be only 0.35 eV higher in energy. This species is equivalent to the most stable isomer $[V^VO_2(\eta^2\text{-}OCH_2)]^-$ of the major product formed in the reaction of $[VO_3]^-$ and methanol (Figure 3b). A number of other isomers were predicted to be about 0.8 eV higher in energy.

Potential-energy surfaces for interaction of $[VO_3]^-$ and CH_3OH: The major product in the reaction of $[VO_3]^-$ and CH_3OH was assigned to $[VO_2(\eta^2\text{-}OCH_2)]^-$ (Figure 3b). Calculations were aimed at addressing the formation of this ion and the minor product ion $[V, O_3, H_2]^-$ (Figure 3a), as well as rationalising the observed isotope labelling and kinetic data for the reaction. The minimum-energy pathway calculated for the reaction of $[VO_3]^-$ with methanol to form $[VO_2(\eta^2\text{-}OCH_2)]^-$ is presented in Figure 4a. The structures of key intermediates are presented in Figure 4b.

The reaction is proposed to proceed via the key intermediates $[VO_2(OH)(OCH_3)]^-$ (**3**) and $[VO(OH)_2(\eta^2\text{-}$

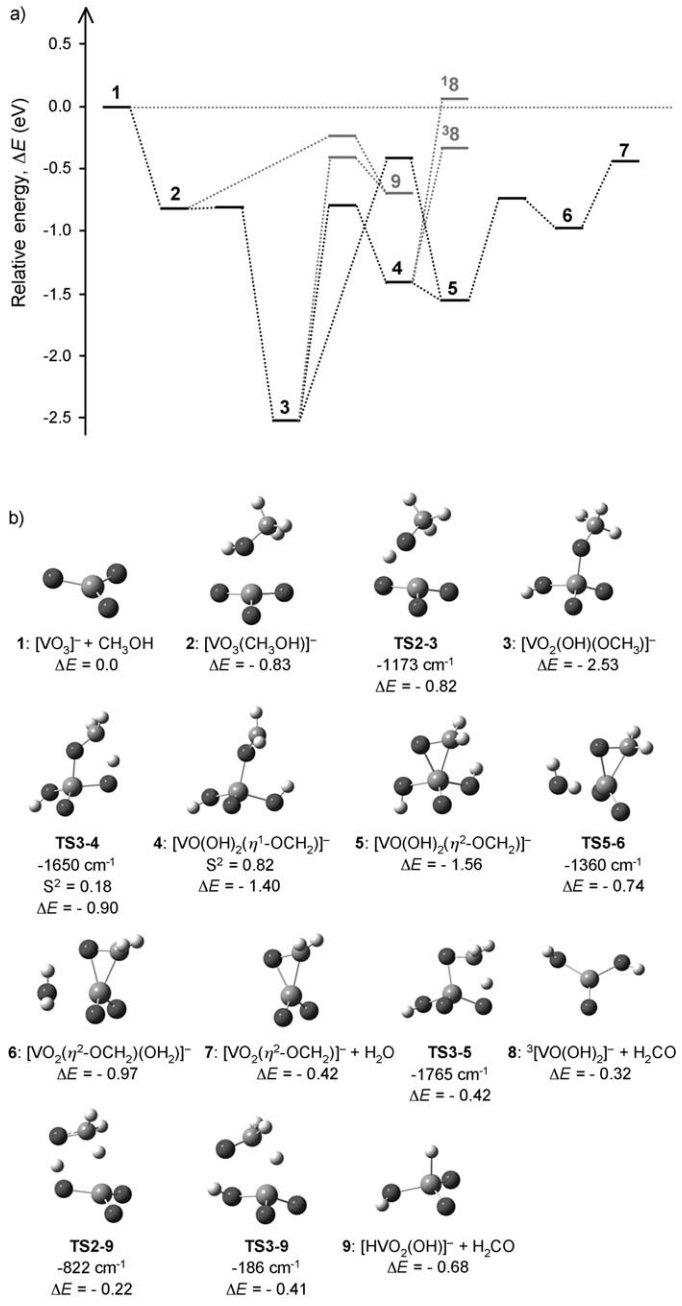

Figure 4. a) Calculated potential-energy surfaces for reaction of $[VO_3]^-$ with CH_3OH. The reaction pathway to form $[VO_2(\eta^2\text{-}OCH_2)]^-$ (**7**) is shown in black, while the pathways to form different isomers of $[V, O_3, H_2]^-$ (**8**, **9**) are shown in grey. b) Structures and energies for key intermediates (minima, transition states). Energies are quoted relative to the separated reactants $[VO_3]^- + CH_3OH$ (relative energy: ΔE, eV).

$OCH_2)]^-$ (**5**), which are interrelated by the formal transfer of a proton from the methoxo ligand of **3** (to form the $[\eta^2\text{-}OCH_2]^{2-}$ ligand) to an oxo ligand (to form a second hydroxo ligand in product **5**; Figure 4b). This might proceed either by direct proton transfer or by intramolecular hydrogen-atom transfer followed by electron transfer. Both pathways were examined theoretically and are described in more detail below. The hydrogen-atom-transfer pathway is predicted to be favoured, and so is described first. The experimental observation of other products [Eq. (1)] is also rationalized by the key intermediates **3** and **5**.

The reaction begins by coordination of methanol to the coordinatively unsaturated metavanadate ion (**1**→**2**), followed by almost barrierless deprotonation of methanol by a terminal oxo ligand (**TS2-3**) to generate $[VO_2(OH)(OCH_3)]^-$ (**3**, Figure 4a). Anion **3** is the most stable species on the potential energy surface. It can undergo intramolecular hydrogen-atom transfer of a methyl hydrogen to a terminal oxo ligand (**TS3-4**) to generate $[VO(OH)_2(\eta^1\text{-}OCH_2)]^-$ (**4**) with an $\eta^1\text{-}O\text{-}OCH_2$ ligand. The transition state **TS3-4** exhibits singlet restricted–unrestricted instability and is spin contaminated ($S^2 = 0.18$), suggesting a single determinant approach is inappropriate. The problem is more pronounced for product **4** ($S^2 = 0.82$), suggesting it is best described as a singlet diradical, that is, a formally $V^{IV}(d^1)$ centre with a ketyl radical-anion ligand, formally $[\eta^1\text{-}OCH_2]^-$. This interpretation is supported by the calculated C–O bond length (e.g. C–O, 1.32 Å; cf. CH_3–OH, 1.42 Å and CH_2=O, 1.20 Å). The η^1-O ligand of **4** can rearrange to the $\eta^2\text{-}O,C$ ligand of $[VO(OH)_2(\eta^2\text{-}OCH_2)]^-$ (**5**), which is predicted to be slightly more stable (Figure 4). We have not attempted to calculate a barrier for this η^1-O to $\eta^2\text{-}O,C$ rearrangement. Proton transfer between the two hydroxo ligands of **5** (**TS5-6**) leads to $[VO_2(\eta^2\text{-}OCH_2)(OH_2)]^-$ (**6**), with a coordinated water molecule, followed by loss of water to form product $[VO_2(\eta^2\text{-}OCH_2)]^-$ (**7**). The C–O bond length in product **7** is consistent with the presence of a formal $V^V(d^0)$ centre and the $[\eta^2\text{-}O,C\text{-}H_2CO]^{2-}$ ligand, isoelectronic with peroxide (C–O, 1.39 Å; cf. CH_3–OH, 1.42 Å and CH_2=O, 1.20 Å). The energies for each of the transition states involved in the transformation **1**→**7** are predicted to be significantly below that of the entrance channel for separated reactants $[VO_3]^- + CH_3OH$ (Figure 4a), consistent with the experimental observation that the reaction occurs at the ion–molecule collision rate.

Alternative pathways for loss of water from intermediate $[VO_2(OH)(OCH_3)]^-$ (**3**) were also examined, including formal proton transfer from the methoxo ligand to an oxo ligand with direct formation of the $[\eta^2\text{-}C,O\text{-}OCH_2]^{2-}$ ligand (**TS3-5**, Figure 4). The transition state for this pathway was predicted as about 0.5 eV higher in energy than that for the hydrogen-atom-transfer pathway described above, and so is not considered further.

A minor product ion at m/z: 101 of stoichiometry $[V, O_3, H_2]^-$ was observed, arising from the formal dehydrogenation of methanol to formaldehyde [Eq. (1a)]. The structure of this ion could not be examined experimentally because of the low intensity in which it was formed (Figure 1). The most stable isomer for product $[V, O_3, H_2]^-$ was predicted to be the hydrido anion $[HVO_2(OH)]^-$ (**9**, Figure 3a). This anion might be formed by concerted hydride and proton transfer from CH_3OH to the metal centre and an oxo ligand of $[VO_3]^-$, respectively (Figure 4b, **TS2-9**). The transition state for this pathway was calculated to be about 0.7 eV higher in energy than that for the hydrogen-atom-transfer

pathway described above (Figure 4a, **TS2-9**). Alternatively, **9** might be formed instead by intramolecular hydride transfer from the coordinated methoxo ligand of intermediate $[VO_2(OH)(OCH_3)]^-$ (**3**) to the metal centre (Figure 4b, **TS3-9**). The transition state for this process is lower than that for direct H^+/H^- transfer (**TS2-9**), but is still about 0.5 eV higher in energy than the hydrogen-atom-transfer pathway.

Singlet and triplet isomers of the dihydroxo centre $[VO(OH)_2]^-$ (^{1}**8** and ^{3}**8**, respectively) were also suggested as isomers for the ion of stoichiometry $[V, O_3, H_2]^-$, and calculated as 0.36 and 0.77 eV higher in energy than the hydrido isomer $[HVO_2(OH)]^-$ (Figure 4a). These might be formed by direct loss of formaldehyde from intermediates $[VO(OH)_2(\eta^1\text{-}OCH_2)]^-$ or $[VO(OH)_2(\eta^2\text{-}OCH_2)]^-$ (**4** or **5**, respectively). Loss of formaldehyde to form singlet $[VO(OH)_2]^-$ (^{1}**8**) is predicted to be higher in energy than the entrance channel $[VO_3]^- + CH_3OH$, and so is not expected to occur (Figure 4a). In contrast, formation of triplet $[VO(OH)_2]^-$ (^{3}**8**) is predicted to be below the energy of the entrance channel, suggesting that this process might be observed experimentally.

Accordingly, the ion at *m*/*z*: 101 of stoichiometry $[V, O_3, H_2]^-$ might be assigned to either the hydrido anion $[HVO_2(OH)]^-$ (**9**) or to triplet $[VO(OH)_2]^-$ (^{3}**8**), both formed by formal dehydrogenation of methanol by $[VO_3]^-$ (Figure 4). The calculations predicted loss of formaldehyde by these pathways to be energetically competitive with that for loss of water to form $[VO_2(\eta^2\text{-}OCH_2)]^-$ (**7**, Figure 4a). However, the latter pathway is significantly favoured experimentally ($\approx$100:1, Figure 1a, compare relative intensities of *m*/*z* 113 and 101). This discrepancy is most likely due to the tight transition state leading to hydride transfer and formation of $[HVO_2(OH)]^-$ (**TS2-9**, Figure 4), as well as loss of formaldehyde from singlet $[VO(OH)_2(OCH_2)]^-$ (**4** or **5**) involving surface crossing to triplet $[VO(OH)_2]^-$ (^{3}**9**) and therefore being hindered kinetically.[48]

Isotope labelling experiments with CD_3OH indicated some exchange of the hydroxyl and methyl hydrogen atoms, resulting in loss of mixtures of DHO/D_2O and $CD_2O/CHDO$ (Figure 1b). The reaction pathway of Figure 4 provides a plausible explanation for these observations. The proposed intermediates **3**, **4** and **5** and the transition states separating them are all predicted to be significantly below the entrance channel $[VO_3]^- + CH_3OH$ and the exit channels for both loss of water or loss of formaldehyde (**7** and ^{3}**8** or **9**, respectively, Figure 4a). This indicates that H/D exchange between methyl and hydroxyl hydrogen atoms should be possible by means of interconversion between intermediates **3** and **4**, for example, for reaction with CD_3OH: $[VO_2(OH)(OCD_3)]^-$ (**3**)$\rightarrow$$[VO(OH)(OD)(\eta^1\text{-}OCD_2)]^-$ (**4**)$\rightarrow$$[VO_2(OD)(OCD_2H)]^-$ (**3′**)$\rightarrow$$[VO(OD)_2(\eta^1\text{-}OCDH)]^-$ (**4′**). Accordingly, formation of H/D exchange intermediates **4** and **4′** accounts for loss of both DHO/CD_2O (from **4**) and $D_2O/CHDO$ (from **4′**).

Potential-energy surfaces for the interaction of $[VO_3]^-$ and CH_3CH_2OH: The major products in the reaction of $[VO_3]^-$ and CH_3CH_2OH were assigned to $[VO_2(OH)_2]^-$ from elimination of ethene and $[V, O_3, C_2, H_4]^-$ from loss of water [Eq. (2)]. The most stable isomer of the latter was predicted to be the anion $[HVO_2(OCH{=}CH_2)]^-$ with a hydrido and a vinoxo ligand, which was 0.35 eV more stable than $[VO_2(\eta^2\text{-}OCHCH_3)]^-$ which features the $[\eta^2\text{-}O,C\text{-}OCHCH_3)]^{2-}$ ligand (Figure 3c). A minor product $[V, O_3, H_2]^-$ was also observed arising from loss of acetaldehyde, and is presumably equivalent to that observed in the methanol reaction. Calculations were aimed at addressing the formation of the major ions $[VO_2(OH)_2]^-$ and $[V, O_3, C_2, H_4]^-$, as well as the likely structure of the latter. The minimum-energy pathway calculated for reaction of $[VO_3]^-$ and ethanol is presented in Figure 5a. The structures of key intermediates (minima, transition states) are presented in Figure 5b.

Similar to the methanol reaction, the major products in the ethanol reaction are proposed to arise from the intermediate alkoxo anion $[VO_2(OH)(OCH_2CH_3)]^-$ (**11**), the most stable species on the potential energy surface (Figure 5). Anion **11** can undergo intramolecular hydrogen-atom transfer to form $[VO(OH)_2(\eta^1\text{-}OCHCH_3)]^-$ (**11**$\rightarrow$**12**), followed by rearrangement to $[VO(OH)_2(\eta^2\text{-}OCHCH_3)]^-$ (**12**$\rightarrow$**13**) and loss of water to form $[VO_2(\eta^2\text{-}OCHCH_3)]^-$ (**13**$\rightarrow$**15**). However, $[HVO_2(OCH{=}CH_2)]^-$ (**16**) was predicted to be 0.35 eV more stable than product $[VO_2(\eta^2\text{-}OCHCH_3)]^-$ (**15**, Figure 3c). Calculations predicted the barrier for conversion of **15** into **16** to be about 1.1 eV (**TS15-16**, Figure 5). However, the formation of **15** from $[VO_3]^- + CH_3CH_2OH$ is predicted to be only weakly exothermic ($\approx$0.4 eV), and so product $[VO_2(\eta^2\text{-}OCHCH_3)]^-$ is unlikely to have sufficient energy for further conversion into $[HVO_2(OCH{=}CH_2)]^-$ (Figure 5). This result indicates that the product ion of stoichiometry $[V, O_3, C_2, H_4]^-$ observed experimentally is likely to be $[VO_2(\eta^2\text{-}C,O\text{-}OCHCH_3)]^-$ (**15**) and not the more stable isomer $[HVO_2(OCH{=}CH_2)]^-$ (**16**).

The alternative product in the ethanol reaction is $[VO_2(OH)_2]^-$ (**17**) arising from loss of ethene [Eq. (2b)]. This might be formed by means of intramolecular β-hydrogen transfer from intermediate $[VO_2(OH)(OCH_2CH_3)]^-$ to an oxo ligand (**TS11-17**, Figure 5). The channel involving loss of ethene is predicted to be favoured thermodynamically over that involving loss of water (products **17** and **15**, respectively, Figure 5). However, the transition state for loss of ethene (**TS11-17**) is predicted to occur at a similar energy to that for hydrogen-atom abstraction to form $[VO(OH)_2(\eta^1\text{-}OCHCH_3)]^-$ (**TS11-12**), as well as that to form $[VO(\eta^1\text{-}OCHCH_3)(OH_2)]^-$ (**TS13-14**) en route to loss of water (Figure 5). The similar energy for these transition states is consistent with the similar branching ratios observed experimentally for these pathways.

Isotope labelling experiments with selectively deuterated ethanol provided insights into the mechanism of reaction. Reaction with CH_3CD_2OH led to exchange of the hydroxyl hydrogen and methylene deuterium atoms prior to loss of water or ethene (e.g. reaction with CH_3CD_2OH resulted in loss of both DHO/D_2O and CH_2CD_2/CH_2CDH). Such exchange is presumably facilitated by a mechanism equivalent

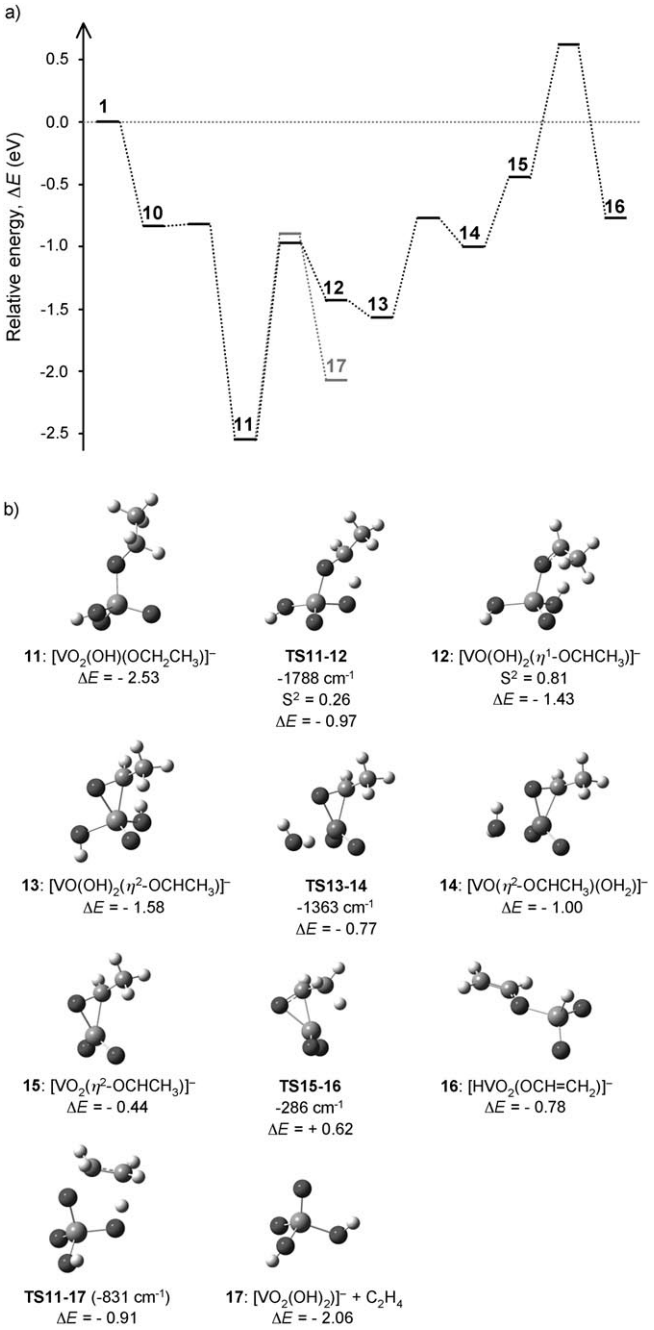

Figure 5. a) Calculated potential-energy surfaces for the reaction of $[VO_3]^-$ with CH_3CH_2OH. The reaction pathway to form $[VO_2(\eta^2\text{-}OCHCH_3)]^-$ (**15**) and then $[HVO_2(OCH{=}CH_2)]^-$ (**16**) is shown in black, while the pathway to form $[VO_2(OH)_2]^-$ (**17**) is shown in grey. b) Structures and energies for key intermediates (minima, transition states). Intermediates in the formation of $[VO_2(OH)(OCH_2CH_3)]^-$ (**11**) are analogous to those for formation of $[VO_2(OH)(OCH_3)]^-$ in the equivalent reaction with CH_3OH (Figure 4), and so are not shown. Energies are relative to the separated reactants $[VO_3]^- + CH_3CH_2OH$ (relative energy: ΔE, eV).

to that proposed for the methanol case above, that is, $[VO_2(OH)(OCD_2CH_3)]^-$ (**11**)→$[VO(OH)(OD)(\eta^1\text{-}OCDCH_3)]^-$ (**12**)→$[VO_2(OD)(OCHDCH_3)]^-$ (**11′**)→$[VO(OD)_2(\eta^1\text{-}OCHCH_3)]^-$ (**12′**). The clean loss of H_2O upon reaction with CD_3CH_2OH (formation of ion at m/z: 130, Figure 2c) confirms that the protons of water originate from the hydroxyl and methylene hydrogen atoms of CD_3CH_2OH, and that methyl hydrogen atoms (deuterium) are not involved in this exchange.

Comparison of the reactivities of $[VO_3]^-$ and $[NbO_3]^-$ towards CH_3OH: The gas-phase reactivity of $[NbO_3]^-$ towards CH_3OH was examined previously by Fourier-transform ion-cyclotron resonance mass spectrometry.[36,49] The major product $[Nb, O_3, H_2]^-$ arose from dehydrogenation [Eq. (3a)]. Dehydration to form $[Nb, O_3, C, H_2]^-$ was a minor pathway only [Eq. (3b)]. This result contrasts with the equivalent reaction for $[VO_3]^-$ described here, in which the major pathway was dehydration, and dehydrogenation was observed as a minor pathway only.

$$[NbO_3]^- \ (m/z:\ 141) + CH_3OH \rightarrow [Nb, O_3, H_2]^- \ (m/z\ 143) + CH_2O \quad (3a)$$

$$\rightarrow [Nb, O_3, C, H_2]^- \ (m/z\ 155) + H_2O \quad (3b)$$

The reactivity of $[NbO_3]^-$ towards CH_3OH was examined theoretically (Figure 6), and may be compared with that of $[VO_3]^-$ (Figure 4). The alkoxo anion $[NbO_2(OH)(OCH_3)]^-$ (**18**) is about 3.2 eV more stable than the separated reactants $[NbO_3]^-$ and CH_3OH, and is again presumed to be the key intermediate in this reaction. Intermediates involved in the formation of **18** are analogous to those for $[VO_2(OH)(OCH_3)]^-$ (**3**, Figure 4), and so are not included in Figure 5. The major pathways for decomposition of **18** were predicted as: 1) transfer of a methyl hydrogen atom to an oxo ligand to directly form $[NbO(OH)_2(\eta^2\text{-}OCH_2)]^-$ (**19**; formally proton transfer, **TS18-19**) and 2) transfer of a methyl hydrogen atom to the Nb centre to form $[HNbO_2(OH)]^-$ (**23**) and formaldehyde (formally hydride transfer, **TS18-23**). Both pathways are shown in Figure 6. Similar pathways were also calculated for $[VO_2(OH)(OCH_3)]^-$ and are included in Figure 4. The favoured pathway for $[VO_2(OH)(OCH_3)]^-$ was predicted to involve hydrogen-atom transfer to initially form $[VO(OH)_2(\eta^1\text{-}OCH_2)]^-$, followed by rearrangement to $[VO(OH)_2(\eta^2\text{-}OCH_2)]^-$ (η^1-O→η^2-C,O) and elimination of water to give product $[VO_2(\eta^2\text{-}OCH_2)]^-$ (**3**→**7**, Figure 4). An equivalent hydrogen-atom transfer pathway for $[NbO_2(OH)(OCH_3)]^-$ was not located, with all attempts instead converging to the proton-transfer pathway for direct formation of $[NbO(OH)_2(\eta^2\text{-}OCH_2)]^-$ (**TS18-19**). This result indicated that the proton-transfer pathway is likely to be favoured over the hydrogen-atom-transfer pathway for $[NbO_2(OH)(OCH_3)]^-$.

Transition states for the proton- or hydride-transfer pathways for $[NbO_2(OH)(OCH_3)]^-$ are approximately equal in energy (i.e. Figure 6, **TS18-19** and **TS18-23**). However, the lowest-energy exit channel is associated with hydride transfer and loss of formaldehyde (**23**+H_2CO). In contrast, exit channels arising from intermediate **19** (following proton transfer) are much higher in energy, for example, **21**+H_2O

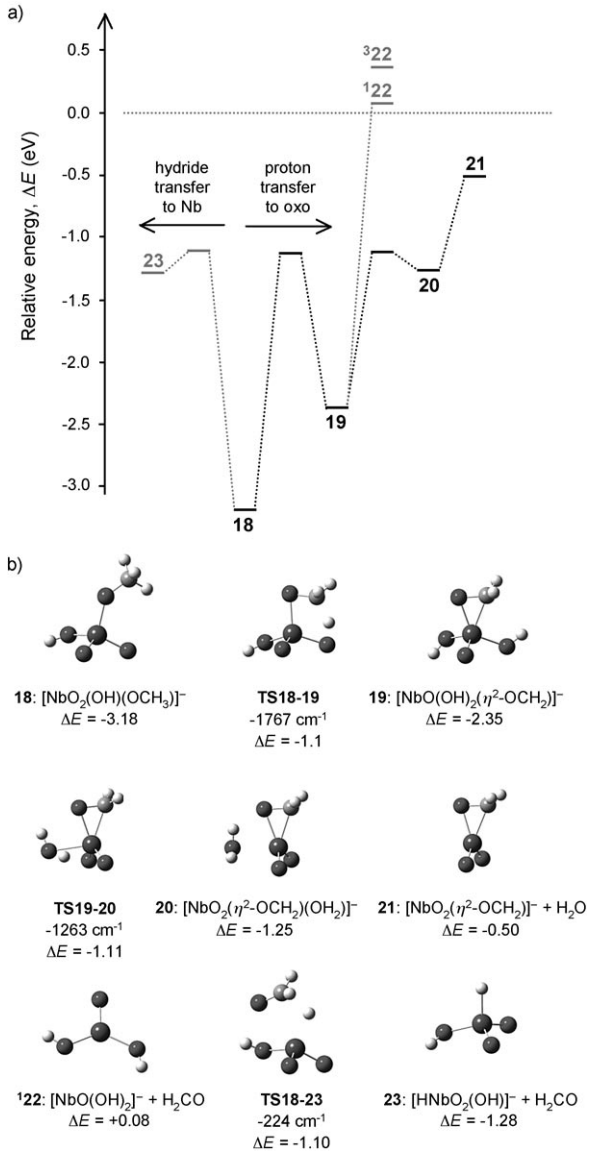

Figure 6. a) Calculated potential-energy surfaces for decomposition of $[NbO_2(OH)(OCH_3)]^-$ (**18**) by means of proton transfer to an oxo ligand or by hydride transfer to the metal centre. The reaction pathway for loss of water to form $[NbO_2(\eta^2\text{-}OCH_2)]^-$ (**21**) is shown in black, while pathways for loss of formaldehyde to form singlet $[NbO(OH)_2]^-$ (**22**) or $[HNbO_2(OH)]^-$ (**23**) are shown in grey. b) Structures and energies for key intermediates (minima, transition states). Energies are relative to the separated reactants $[NbO_3]^- + CH_3OH$ (relative energy: ΔE, eV).

or ^{1}**22** + CH_2O. This finding indicated that hydride transfer to form **23** + CH_2O should be preferred for $[NbO_2(OH)(OCH_3)]^-$. The theoretical preference for hydride transfer is in agreement with the experimental results, in which the dominant product ion was $[Nb, O_3, H_2]^-$ from dehydrogenation of methanol to formaldehyde.[36] This earlier study assigned product $[Nb, O_3, H_2]^-$ to the dihydroxy centre $[NbO(OH)_2]^-$ (**22**). However, the present calculations suggest that the alternative hydride isomer $[HNbO_2(OH)]^-$ (**23**) is favoured on both kinetic and thermodynamic grounds.

Comparison with previous theoretical results: The mechanism of alcohol oxidation at oxovanadium fragments has been examined previously.[31,32,40,50] Model systems ranged from mononuclear vanadate centres, such as $[VO(OCH_3)_3]$, to larger systems designed to mimic supported vanadate centres (for example, $[VO\{OM(OH)_3\}_3]$; M: Si, Ti, Zr). The consensus mechanism involves condensation of CH_3OH at a vanadium centre to form a $V^VO(OCH_3)$ fragment, followed by *net* transfer of a proton and two electrons from the methoxo ligand to generate a $V^{III}(OH)$ fragment and formaldehyde. Recent studies on the model system $[VO(OCH_3)_3]$ suggest that the latter step occurs by formal hydrogen-atom transfer via a biradical intermediate $[V^{IV}(OH)(OCH_2)(OCH_3)_2]$ (Scheme 2a).[40] This can decompose further by loss of formaldehyde to form triplet $[V^{III}(OH)(OCH_3)_2]$. $[VO_2(OH)(OCH_3)]^-$ of the present study was also proposed to undergo an equivalent hydrogen-atom transfer (Scheme 2b). However, the present experiments indicate that product $[V^{IV}O(OH)_2(\eta^1\text{-}OCH_2)]^-$ does not dissociate by loss of formaldehyde, but rather by loss of water to form $[VO_2(\eta^2\text{-}OCH_2)]^-$. This alternative reaction is presumably favoured, as the intersystem crossing necessary for loss of formaldehyde is avoided (i.e. singlet $[VO(OH)_2(\eta^1\text{-}OCH_2)]^-$ to triplet $[VO(OH)_2]^-$).

The relevance of a previous gas-phase study on the radical cation $[VO(OCH_3)_3]^+$ was questioned on the basis of the significant electronic differences between cation $[VO(OCH_3)_3]^+$ and neutral $VO(OCH_3)_3$.[40] The major differences were: 1) the transition state for hydrogen transfer in cation $[OV(OCH_3)_3]^+$ was stabilized significantly due to the presence of a radical methoxo ligand, 2) the reaction for $[OV(OCH_3)_3]^+$ was more exothermic due to the formation of a stable V^{IV} product centre (cationic $[V^{IV}(OH)(OCH_3)_2]^+$ rather than neutral $[V^{III}(OH)(OCH_3)_2]$, and 3) the entire reaction for $[VO(OCH_3)_3]^+$ can proceed on the doublet surface, without the need for surface crossing. These problems are avoided in the present work for $[VO_2(OH)(OCH_3)]^-$ (Scheme 2b) as: 1) it is a closed-shell singlet molecule, 2) the product from loss of formaldehyde is the V^{III} centre $[V^{III}O(OH)_2]^-$, and 3) surface crossing is required for loss of formaldehyde to form triplet $[V^{III}O(OH)_2]^-$. Accordingly, the experimentally observed loss of water from intermediate $[VO_2(OH)(OCH_3)]^-$ reinforces the importance of competing pathways in the reactions of $VO(OCH_3)$ fragments and the role of spin and coordination environment in determining reactivity.

Hydrogen-atom transfer pathways have been proposed previously as the initial step in the oxidation of hydrocarbons by a number of high-valent metal oxo reagents, for example, MnO_4^- and RuO_4.[51–53] The reactions proceed by transfer of H^+ to an oxo ligand and e^- to the metal centre, that is, proton-coupled electron transfer. The intramolecular hydrogen-atom transfer pathways proposed here for $[VO_2(OH)(OCH_3)]^-$ and previously for $[VO(OCH_3)_3]$[40] are equivalent intramolecular processes. In these cases, protonation of an oxo ligand and $1e^-$ reduction of the V^V centre generates a stable V^{IV} centre with a coordinated ketyl radi-

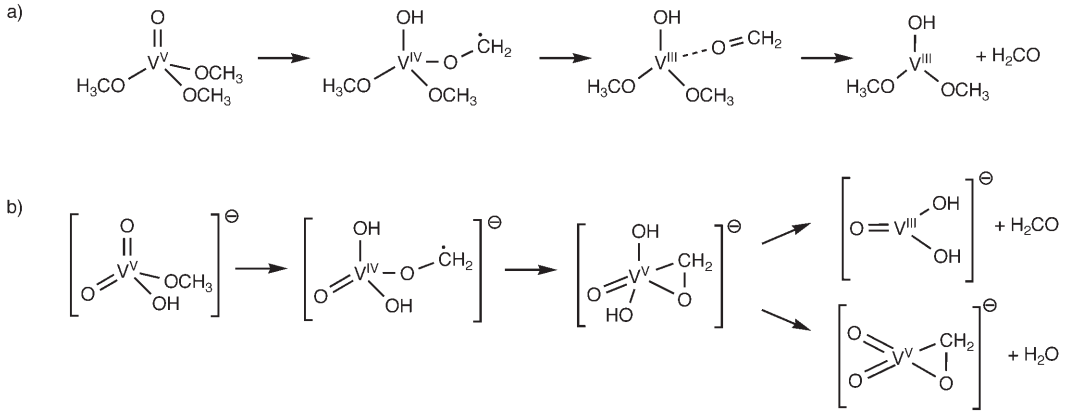

Scheme 2.

cal-anion ligand (e.g. $[V^{IV}O(OH)_2(\eta^1\text{-}OCH_2)]^-$; Figure 4, Scheme 2b). This ligand can then either dissociate as the aldehyde (e.g. to form $[V^{III}O(OH)_2]^-$) or remain bound to the metal centre, allowing for an alternative reaction to occur (e.g. loss of water to form $[V^{IV}O_2(\eta^2\text{-}OCH_2)]^-$).

The $[\eta^2\text{-}O,C\text{-}OCHR]^{2-}$ ligands proposed for $[VO_2(\eta^2\text{-}OCH_2)]^-$ and $[VO_2(\eta^2\text{-}OCHCH_3)]^-$ have been observed previously for some related organometallic species.[54] For example, the complex $Cp_2V(\eta^2\text{-}O,C\text{-}OCH_2)$ (Cp: $\eta^5\text{-}C_5H_5$) was prepared by reaction of paraformaldehyde with vanadocene Cp_2V.[55,56] Equivalent ligands have been observed for the heavier congeners niobium and tantalum,[57,58] as well as for siloxide-supported centres, for example, $[(t\text{Bu}_3\text{SiO})_3\text{Ta}(\eta^2\text{-}O,C\text{-}OCH_2)]$.[59–61] Such complexes are relevant to the catalytic reduction of carbon monoxide, for which coordinated $\eta^2\text{-}O,C\text{-}OCH_2$ ligands are possible intermediates.[54,56,58] The present work demonstrates the formation of a $\eta^2\text{-}O,C\text{-}OCH_2$ ligand at a vanadium centre by hydrogen-atom transfer from a methoxo ligand.

The present gas-phase reactions might be relevant to the reactivity of alcohols at supported mononuclear vanadium oxide sites.[5,62] Recent studies suggest that such sites involve isolated tetrahedral M–$VO(OH)_2$ fragments that are proposed to undergo condensation with methanol to generate M–$VO(OH)(OCH_3)$ species (M: catalyst support, e.g. SiO_2, Al_2O_3, Nb_2O_5, ZrO_2).[62] The methoxo ligand of the latter may then be oxidized and lost as formaldehyde. Intermediate $[VO_2(OH)(OCH_3)]^-$ of the present work is structurally similar to these M–$VO(OH)(OCH_3)$ fragments, suggesting its reactivity might be relevant. In particular, a mechanism similar to the hydrogen-atom transfer pathway proposed for $[VO_2(OH)(OCH_3)]^-$ to generate a $\eta^2\text{-}C,O$ ligand might also occur at supported vanadium oxide sites. Such intermediates may dissociate through loss of formaldehyde or water, as observed in the present work, or undergo further decomposition. Preliminary studies indicate that collisional activation of $[VO_2(\eta^2\text{-}OCH_2)]^-$ results in decomposition by means of decarbonylation to form the dihydride $[(H)_2VO_2]^-$ [Eq. (4)], suggesting a possible role of such $\eta^2\text{-}C,O$ ligands in the overoxidation of methanol to carbon monoxide.

$$[VO_2(\eta^2\text{-}OCH_2)]^-\ (m/z:\ 113) \rightarrow [(H)_2VO_2]^-\ (m/z:\ 85) + CO \quad (4)$$

Conclusions

The gas-phase reactivity of the metavanadate anion $[VO_3]^-$ towards methanol was examined by multistage mass spectrometry experiments and DFT calculations. $[VO_3]^-$ dehydrated methanol to eliminate water and form $[VO_2(\eta^2\text{-}OCH_2)]^-$, which features an $[\eta^2\text{-}C,O\text{-}OCH_2]^{2-}$ ligand formed by formal removal of two protons from methanol and which is isoelectronic with peroxide. Theoretical calculations indicated that the reaction occurs by addition of methanol to form the methoxo anion $[VO_2(OH)(OCH_3)]^-$, followed by hydrogen-atom transfer to form $[VO(OH)_2(\eta^1\text{-}OCH_2)]^-$. The rearrangement $\eta^1\text{-}O \rightarrow \eta^2\text{-}C,O$ then occurs to form $[VO(OH)_2(\eta^2\text{-}OCH_2)]^-$. The latter may eliminate water or aldehyde to generate products $[V^VO_2(\eta^2\text{-}OCHR)]^-$ or $[V^{III}O(OH)_2]^-$, respectively, with loss of water dominating experimentally. Equivalent reactions were also observed for ethanol, as well as dehydration to form $[VO_2(OH)_2]^-$ and ethene. The major product observed in the reaction of $[VO_3]^-$ with methanol is different from that observed for the heavier niobium analogue $[NbO_3]^-$ described previously. The latter dehydrogenated methanol to form an ion of stoichiometry $[Nb, O_3, H_2]^-$. The present calculations indicate that this occurs by means of hydride transfer from intermediate $[NbO_2(OH)(OCH_3)]^-$ to form $[HNbO_2(OH)]^-$. Comparisons of the present work with previous studies suggest that $[\eta^2\text{-}C,O\text{-}OCHR]^{2-}$ ligands should be considered as plausible intermediates in a number of catalytic processes occurring at vanadium oxide centres.

Experimental Section

Reagents: CH_3OH (HPLC grade) and CD_3OH (99 atom % D) were obtained from Aldrich and used without further purification. $CH_3{}^{18}OH$ (95 atom % ^{18}O) was obtained from Isotec. CH_3CH_2OH (HPLC grade), CD_3CH_2OH (98 atom % D), CH_3CD_2OH (98 atom % D) and

CD_3CD_2OD (99.5 atom % D) were obtained from Aldrich and used without further purification.

Mass spectrometry: Mass spectrometry experiments were conducted with a modified Finigan LCQ quadrupole ion-trap mass spectrometer equipped with a Finnigan electrospray ionization source. Mass selection and collisional activation were carried out by using standard isolation and excitation procedures and the "advanced scan" function of the LCQ software. The instrument was modified to permit introduction of neutral reagents into the ion trap, thus allowing the measurement of ion–molecule reaction rate constants. The modifications and experimental procedure have been described in detail previously.[47] Reaction efficiencies (φ) were calculated by dividing the experimentally determined rate constant (k_{exp}) by theoretical predictions of ion–molecule collision rate constants (k_{ado}).[63]

Theoretical calculations: DFT calculations were carried out with the hybrid B3LYP functional,[64,65] by using the Gaussian 03 program.[66] The B3LYP functional has been used previously for a range of vanadium oxide systems, and was shown to give reasonable agreement with available experimental data as well as with higher-level theoretical calculations.[19,20,23,24,27,31,32,67–70] Calculations were carried out by using the 6-311$^+$ $^+$G** basis sets for H, C and O, and the SDD effective core potential (ECP) and associated basis sets were used for V.[71] The use of an ECP basis set for V was chosen to allow for direct comparison with the heavier Nb centres. Stationary points were characterized by frequency calculations, and unscaled zero-point energies are included for all species. Cartesian coordinates and energies of optimized geometries are included in the Supporting Information.

An important reaction pathway in the interaction of $[VO_3]^-$ and alcohols involved hydrogen-atom transfer, and intermediates for these pathways exhibited singlet restricted–unrestricted instabilities, indicating problems with the single determinant wavefunction. These intermediates were approximately modelled by the broken-symmetry DFT approach,[72–75] based on a procedure used previously for related vanadium oxide centres that were proposed to react by similar hydrogen-atom transfer pathways.[20,40] Projected low-spin energies for broken-symmetry solutions were obtained by spin-projection methods from single-point triplet and broken-symmetry singlet energies at the broken-symmetry singlet geometries; the energies used in these calculations are detailed in the Supporting Information.[20,40,74,75] Spin expectation values S^2 are indicated in the text for these species where appropriate.

Acknowledgements

T.W., A.G.W. and R.A.J.O. thank the Australian Research Council for financial support by grants #DP0772053, #DP0450134 and #DP0558430, respectively. T.W. thanks the Victorian Institute for Chemical Sciences High-Performance Computing Facility for allocation of computer time. R.A.J.O. thanks the ARC Centres of Excellence program (ARC Centre of Excellence in Free Radical Technology and Biotechnology).

[1] See for example: a) G. Centi, F. Cavani, F. Trifirò, *Selective Oxidation by Heterogeneous Catalysis*, Kluwer Academic, New York, **2001**, p. 505; b) J. M. Thomas, W. J. Thomas, *Principles and Practice of Heterogeneous Catalysis*, Wiley-VCH, Weinheim, **1996**, p. 669.
[2] a) G. Centi, S. Perathoner, *Int. J. Mol. Sci.* **2001**, *2*, 183–196; b) R. K. Grasselli, *Top. Catal.* **2002**, *21*, 79–88.
[3] G. C. Bond, S. F. Tahir, *Appl. Catal.* **1991**, *71*, 1–31
[4] *Appl. Catal. A* **1997**, *157*, 1–425 (special issue devoted to vanadia catalysts for selective oxidation of hydrocarbons and their derivatives).
[5] B. M. Weckhuysen, *Catal. Today* **2003**, *78*, 25–46.
[6] A. Butler, M. J. Clague, G. E. Meister, *Chem. Rev.* **1994**, *94*, 625–638.
[7] T. Hirao, *Chem. Rev.* **1997**, *97*, 2707–2724.
[8] K. Dyrek, M. Che, *Chem. Rev.* **1997**, *97*, 305–331.
[9] R. K. Grasselli, *Top. Catal.* **2002**, *21*, 79–88.
[10] J. C. Vedrine, *Top. Catal.* **2002**, *21*, 97–106.
[11] U. S. Ozkan, R. B. Watson, *Catal. Today* **2005**, *100*, 101–114.
[12] K. A. Zemski, D. R. Justes, A. W. Castleman, Jr., *J. Phys. Chem. B* **2002**, *106*, 6136–6148.
[13] D. K. Böhme, H. Schwarz, *Angew. Chem.* **2005**, *117*, 2388–2406; *Angew. Chem. Int. Ed.* **2005**, *44*, 2336–2354.
[14] A. Dinca, T. P. Davis, K. J. Fisher, D. R. Smith, G. D. Willett, *Int. J. Mass Spectrom.* **1999**, *182–183*, 73–84.
[15] A. Dinca, T. P. Davis, K. J. Fisher, D. R. Smith, G. D. Willett, *Int. J. Mass Spectrom.* **2000**, *194*, 209–224.
[16] K. A. Zemski, D. R. Justes, A. W. Castleman, Jr., *J. Phys. Chem. A* **2001**, *105*, 10237–10245.
[17] M. Engeser, M. Schlangen, D. Schröder, H. Schwarz, T. Yumura, K. Yoshizawa, *Organometallics* **2003**, *22*, 3933–3943.
[18] S. Feyel, D. Schröder, H. Schwarz, *J. Phys. Chem. A* **2006**, *110*, 2647–2654.
[19] S. Feyel, J. Döbler, D. Schröder, J. Sauer, H. Schwarz, *Angew. Chem.* **2006**, *118*, 4797–4801; *Angew. Chem. Int. Ed.* **2006**, *45*, 4681–4685.
[20] S. Feyel, D. Schröder, X. Rozanska, J. Sauer, H. Schwarz, *Angew. Chem.* **2006**, *118*, 4793–4797; *Angew. Chem. Int. Ed.* **2006**, *45*, 4677–4681.
[21] R. C. Bell, K. A. Zemski, K. P. Kerns, H. T. Deng, A. W. Castleman, Jr., *J. Phys. Chem. A* **1998**, *102*, 1733–1742.
[22] R. C. Bell, A. W. Castleman, Jr., *J. Phys. Chem. A* **2002**, *106*, 9893–9899.
[23] D. R. Justes, R. Mitric, N. A. Moore, V. Bonacic-Koutecky, A. W. Castleman, Jr., *J. Am. Chem. Soc.* **2003**, *125*, 6289–6299.
[24] N. A. Moore, R. Mitric, D. R. Justes, V. Bonacic-Koutecky, A. W. Castleman, Jr., *J. Phys. Chem. B* **2006**, *110*, 3015–3022.
[25] D. R. Justes, N. A. Moore, A. W. Castleman, Jr., *J. Phys. Chem. B* **2004**, *108*, 3855–3862.
[26] Y. Cao, X. Zhao, B. Xin, S. Xiong, Z. Tang, *J. Mol. Struct.* **2004**, *683*, 141–146.
[27] M. Engeser, D. Schröder, H. Schwarz, *Chem. Eur. J.* **2005**, *11*, 5975–5987.
[28] T. Waters, G. N. Khairallah, S. A. S. Y. Wimala, Y. C. Ang, R. A. J. O'Hair, A. G. Wedd, *Chem. Commun.* **2006**, 4503–4505.
[29] K. A. Zemski, A. W. Castleman, Jr., D. L. Thorn, *J. Phys. Chem. A* **2001**, *105*, 4633–4639.
[30] D. Schröder, M. Engeser, M. Bronstrup, C. Daniel, J. Spandl, H. Hartl, *Int. J. Mass Spectrom.* **2003**, *228*, 743–757.
[31] D. Schröder, J. Loos, M. Engeser, H. Schwarz, H.-C. Jankowiak, R. Berger, R. Thissen, O. Dutuit, J. Döbler, J. Sauer, *Inorg. Chem.* **2004**, *43*, 1976–1985.
[32] D. Schröder, M. Engeser, H. Schwarz, E. C. E. Rosenthal, J. Döbler, J. Sauer, *Inorg. Chem.* **2006**, *45*, 6235–6245.
[33] K. A. Zemski, R. C. Bell, A. W. Castleman, Jr., *Int. J. Mass Spectrom.* **1999**, *184*, 119–128.
[34] K. A. Zemski, R. C. Bell, A. W. Castleman, Jr., *J. Phys. Chem. A* **2000**, *104*, 5732–5741.
[35] K. A. Zemski, D. R. Justes, R. C. Bell, A. W. Castleman, Jr., *J. Phys. Chem. A* **2001**, *105*, 4410–4417.
[36] P. Jackson, K. J. Fisher, G. D. Willett, *Int. J. Mass Spectrom.* **2000**, *197*, 95–103.
[37] P. Jackson, K. J. Fisher, G. D. Willett, *Chem. Phys.* **2000**, *262*, 179–187.
[38] I. Nowak, M. Ziolek, *Chem. Rev.* **1999**, *99*, 3603–3624.
[39] M. Ziolek, *Catal. Today* **2003**, *78*, 47–64.
[40] J. Doebler, M. Pritzsche, J. Sauer, *J. Am. Chem. Soc.* **2005**, *127*, 10861–10868.
[41] L. Gracia, J. Andres, V. S. Safont, A. Beltran, J. R. Sambrano, *Organometallics* **2004**, *23*, 730–739.
[42] L. Gracia, J. R. Sambrano, J. Andres, A. Beltran, *Organometallics* **2006**, *25*, 1643–1653.
[43] O. Bortolini, M. Carraro, V. Conte, S. Moro, *Eur. J. Inorg. Chem.* **1999**, 1489–1495.

[44] M. Bonchio, O. Bortolini, V. Conte, S. Primon, *J. Chem. Soc. Perkin Trans. 2* **2001**, 763–765.
[45] M. Bonchio, O. Bortolini, V. Conte, S. Moro, *Eur. J. Inorg. Chem.* **2001**, 2913–2919.
[46] O. Bortolini, V. Conte, *J. Inorg. Biochem.* **2005**, *99*, 1549–1557.
[47] T. Waters, R. A. J. O'Hair, A. G. Wedd, *J. Am. Chem. Soc.* **2003**, *125*, 3384–3396.
[48] H. Schwarz, *Int. J. Mass Spectrom.* **2004**, *237*, 75–105.
[49] [NbO_3^-] was previously generated by laser vaporization of Nb_2O_5 (ref. [36]). We have also attempted to generate this ion by electrospray but, despite repeated attempts, have not been successful.
[50] R. Z. Khaliullin, A. T. Bell, *J. Phys. Chem. B* **2002**, *106*, 7832–7838.
[51] J. M. Mayer, *Acc. Chem. Res.* **1998**, *31*, 441–450.
[52] C. Limberg, *Angew. Chem.* **2003**, *115*, 6112–6136; *Angew. Chem. Int. Ed.* **2003**, *42*, 5932–5954.
[53] J. M. Mayer, E. A. Mader, J. P. Roth, J. R. Bryant, T. Matsuo, A. Dehestani, B. C. Bales, E. J. Watson, T. Osako, K. Valliant-Saunders, W. H. Lam, D. A. Hrovat, W. T. Borden, E. R. Davidson, *J. Mol. Catal. A* **2006**, *251*, 24–33.
[54] Y. H. Huang, J. A. Gladysz, *J. Chem. Educ.* **1988**, *65*, 298–303.
[55] S. Gambarotta, C. Floriani, A. Chiesi-Villa, C. Guastini, *J. Am. Chem. Soc.* **1982**, *104*, 2019–2020.
[56] S. Gambarotta, C. Floriani, A. Chiesi-Villa, C. Guastini, *Organometallics* **1986**, *5*, 2425–2433.
[57] A. Van Asselt, B. J. Burger, V. C. Gibson, J. E. Bercaw, *J. Am. Chem. Soc.* **1986**, *108*, 5347–5349.
[58] B. Thiyagarajan, L. Michalczyk, J. C. Bollinger, J. C. Huffman, J. W. Bruno, *Organometallics* **1996**, *15*, 1989–1999.
[59] R. E. LaPointe, P. T. Wolczanski, J. F. Mitchell, *J. Am. Chem. Soc.* **1986**, *108*, 6382–6384.
[60] R. E. LaPointe, P. T. Wolczanski, *J. Am. Chem. Soc.* **1986**, *108*, 3535–3537.
[61] P. T. Wolczanski, *Polyhedron* **1995**, *14*, 3335–3362.
[62] D. E. Keller, S. M. K. Airaksinen, A. O. Krause, B. M. Weckhuysen, D. C. Koningsberger, *J. Am. Chem. Soc.* **2007**, *129*, 3189–3197.
[63] K. F. Lim, *Quantum Chem. Program Exchange Bull.* **1994**, *14*, 3.
[64] A. D. Becke, *J. Chem. Phys.* **1993**, *98*, 5648–5652.
[65] C. Lee, W. Yang, R. G. Parr, *Phys. Rev. B* **1988**, *37*, 785–789.
[66] Gaussian 03 (Revision B.04), M. J. Frisch, G. W. Trucks, H. B. Schlegel, G. E. Scuseria, M. A. Robb, J. R. Cheeseman, J. A. Montgomery, Jr., T. Vreven, K. N. Kudin, J. C. Burant, J. M. Millam, S. S. Iyengar, J. Tomasi, V. Barone, B. Mennucci, M. Cossi, G. Scalmani, N. Rega, G. A. Petersson, H. Nakatsuji, M. Hada, M. Ehara, K. Toyota, R. Fukuda, J. Hasegawa, M. Ishida, T. Nakajima, Y. Honda, O. Kitao, H. Nakai, M. Klene, X. Li, J. E. Knox, H. P. Hratchian, J. B. Cross, V. Bakken, C. Adamo, J. Jaramillo, R. Gomperts, R. E. Stratmann, O. Yazyev, A. J. Austin, R. Cammi, C. Pomelli, J. W. Ochterski, P. Y. Ayala, K. Morokuma, G. A. Voth, P. Salvador, J. J. Dannenberg, V. G. Zakrzewski, S. Dapprich, A. D. Daniels, M. C. Strain, O. Farkas, D. K. Malick, A. D. Rabuck, K. Raghavachari, J. B. Foresman, J. V. Ortiz, Q. Cui, A. G. Baboul, S. Clifford, J. Cioslowski, B. B. Stefanov, G. Liu, A. Liashenko, P. Piskorz, I. Komaromi, R. L. Martin, D. J. Fox, T. Keith, M. A. Al-Laham, C. Y. Peng, A. Nanayakkara, M. Challacombe, P. M. W. Gill, B. Johnson, W. Chen, M. W. Wong, C. Gonzalez, J. A. Pople, Gaussian, Inc., Wallingford, CT, **2004**.
[67] S. F. Vyboishchikov, J. Sauer, *J. Phys. Chem. A* **2000**, *104*, 10913–10922.
[68] M. Pykavy, C. van Wullen, J. Sauer, *J. Chem. Phys.* **2004**, *120*, 4207–4215.
[69] J. Sauer, J. Doebler, *Dalton Trans.* **2004**, 3116–3121.
[70] K. R. Asmis, G. Santambrogio, M. Bruemmer, J. Sauer, *Angew. Chem.* **2005**, *117*, 3182–3185; *Angew. Chem. Int. Ed.* **2005**, *44*, 3122–3125.
[71] M. Dolg, U. Wedig, H. Stoll, H. Preuss, *J. Chem. Phys.* **1987**, *86*, 866–872.
[72] L. Noodleman, *J. Chem. Phys.* **1981**, *74*, 5737–5743.
[73] J. Li, L. Noodleman, D. A. Case in *Inorganic Electronic Structure and Spectroscopy, Vol. I: Methodology* (Eds.: E. I. Solomon, A. B. P. Lever), Wiley, New York, **1999**, pp. 661–724.
[74] R. Caballol, O. Castell, F. Illas, I. de Moreira, J. P. Malrieu, *J. Phys. Chem. A* **1997**, *101*, 7860–7866.
[75] J. Graefenstein, A. M. Hjerpe, E. Kraka, D. Cremer, *J. Phys. Chem. A* **2000**, *104*, 1748–1761.

Received: April 24, 2007
Revised: June 5, 2007
Published online: July 27, 2007

